

Head-Discharge Equation for Dam Breach: Three-Dimensional Numerical Study on 1:1 Scale

I. R. V. Gama¹, A. L. A. Simões²

^{1,2}Federal University of Bahia, Salvador, Bahia, 40210-630, Salvador, Brazil

Corresponding Author: andre.simo@ufba.br

Abstract

During the gradual breach of a dam, breaches with irregular shapes may form. Various models exist for establishing rupture scenarios, incorporating different formulations for the relationship between the flow through the breach and its corresponding hydraulic head. These formulations often adopt power-law forms with exponents akin to those observed in triangular, trapezoidal, or parabolic weirs. The present study seeks to analyze the exponent values within this context through three-dimensional prototype-scale simulations employing computational fluid dynamics (CFD). For the simulation of flow through three breaches, with dimensions closely resembling those of the Teton Dam, the Reynolds-averaged Navier-Stokes equations and mass conservation were employed. The inhomogeneous model and the $k-\epsilon$ turbulence model were applied. The results obtained for the relationship between flow rate and hydraulic head exhibited behavior that could be approximated with a power-law, akin to spillways. When considering individual dam breaches, the values of exponents closely approximated those observed in triangular weirs for the two smaller breaches. However, for the largest breach, or when considering a unified analysis of all numerical results, the exponent converged to approximately three.

Keywords: CFD, dam breach, dam failure, Discharge-head equation, hydraulics.

Date of Submission: 10-03-2024

Date of acceptance: 23-03-2024

I. INTRODUCTION

Historically, it is well-established that dams have risks associated with their structural integrity. According to Singh (1996), between 1802 and 1980, twenty-three dam failures occurred worldwide, resulting in the loss of 8,655 human lives. In order to define emergency procedures in case of accidents, hypothetical breach scenarios must be simulated using computational modeling. For earthen dams, breaches can occur with the formation of piping and gaps caused by structural failures or overtopping. As an essential part of modeling, rupture scenarios and possible approximations for the shapes of piping and gaps are conceived, enabling the calculation of the effluent hydrograph from the reservoir for subsequent simulation of the flood wave propagation downstream of the dam and prediction of its consequences.

According to Singh and Snorrason (1982), the duration of earthen dam breaches can range from fifteen minutes to five hours. Ponce (1982) observed that such duration can vary from 3 to 12 hours. During the dam breach process, piping may occur, evolving temporally towards the crest. The fragility resulting from this phenomenon facilitates crest rupture and the formation of one or more gaps, as observed in the case of the Teton Dam, described by Singh (1996).

According to MacDonald and Langridge-Monopolis (1984), based on historical failure analyses, gaps in earthfill dams assume approximately triangular shapes with a 2V:1H ratio, provided the rupture evolves to the base. The same authors note that if erosion of the base material occurs, the shape may become trapezoidal, maintaining slopes with a 2V:1H ratio. Houston (1985), analyzing data from MacDonald and Langridge-Monopolis (1984), concluded that the gap's shape is trapezoidal with a 1V:1V ratio, with the base width equal to the gap's height, suggesting a potential divergence in the definition of the shape.

Understanding the possible shapes of dam breach led to the proposition of approximations for the relationship between flow rate, Q , and hydraulic head, h , as seen in Cristofano (1965), who proposed the use of a relationship similar to that of thick-walled trapezoidal weirs, with Q proportional to $h^{3/2}$, and in Harris and Wagner (1967), who suggest the use of a parabolic breach, with Q proportional to $h^{5/2}$, a condition also corresponding to the triangular shape. The Fread model (1984a, b), known as DAMBRK, assumes that the flow rate is proportional to the sum of two terms, one with $h^{3/2}$ and another with $h^{5/2}$.

Wetmore and Fread (1984) developed a simplified version of DAMBRK, named SMPDBK, useful at that time due to the unavailability of computers for more detailed rapid analyses. It is a simplification that assumes the gap as rectangular or, approximately, trapezoidal when using the average width of the trapezoid.

With the evolution of computers, it is currently possible to perform calculations without such simplifications relatively quickly. In this context, models have evolved to use one-dimensional Saint-Venant equations coupled with sediment transport models, vertically integrated Navier-Stokes and mass conservation equations in two dimensions, and for specific studies on rupture characteristics, with three-dimensional Navier-Stokes and mass conservation equations, employing Reynolds averages and turbulence models.

Between 1987 and 2020, at least twelve articles were published on the subject in major international Hydraulic journals. Table 1 summarizes the main contributions of these works and shows that only three studies employed computational fluid dynamics, with two conducting simulations in three dimensions.

Table 1: Summary of studies on dam break.

Authors	Contribution
Wurbs (1987)	Comparison using different models applied to two rupture cases. The author concluded that the SMPDBK model corresponded to optimal modeling.
Singh and Quiroga (1988)	Dimensionless modeling for erosion, based on ordinary differential equation and analytical solution for it, with sensitivity analysis of the model using applications.
Gozali and Hunt (1993)	Numerical solution of the Saint-Venant equations for the wave inside the reservoir, based on the partial formation of a breach.
Ponce <i>et al.</i> (2003)	Dimensionless analytical solution for the 1D shallow water equations from the corresponding perturbation equations.
Wahl (2004)	Quantification of uncertainties of different methods designed to predict the breach formation and corresponding peak flows.
Franca and Almeida (2004)	Carrying out experiments and modeling of rockfill dam failure.
Froehlich (2008)	Analysis of data from 74 rupture cases to propose models for the width of the breach and its inclination, considering the trapezoidal shape, as a function of time.
Biscarini <i>et al.</i> (2010)	Comparison between the shallow water equations in 2D with the Navier-Stokes equations with Reynolds averages, mass conservation and the k-ε turbulence model, in 3D.
Tao and Tao (2017)	Study of piping formation through the coupling of computational fluid dynamics with the discrete element method, to simulate erosion.
Tabrizi <i>et al.</i> (2017)	Proposition of a simplified model for the formation of triangular breach from different degrees of compaction.
Kaurav <i>et al.</i> (2019)	2D modeling of the overtopping and erosion of a dam, using the Reynolds Averaged Navier-Stokes equations (RANS), mass conservation and the k-ε turbulence model, with the sediment transport model available in the FLOW-3D software.
Amaral <i>et al.</i> (2020)	Proposal and study of procedures for experimental studies of breaches and earth dams due to overtopping.

The present work aimed to study the relationship between flow from breaches and its corresponding hydraulic head. To carry out the research, three breaches with shapes approximately similar to the breaches observed with the temporal evolution of the Teton dam rupture were studied. The following specific objectives were established: (1) determine the exponents of the flow – hydraulic head equation for each of the three breaches and compare them to literature models; (2) calculate a single exponent of the flow – hydraulic head equation, considering the results of simulations carried out with the three breaches in an integrated manner.

II. MATERIAL AND METHODS

2.1 Teton Dam failure and definition of breaches

The Teton Dam, constructed between 1972 and 1975 in Idaho, USA, experienced a rupture in 1976 during its initial filling. The rupture initiated from the formation of small mud seepages that evolved into piping, progressing towards the crest, eventually breaching it and forming a gap, as described by Jansen (1988), Hager *et al.* (2021, p.956), and photographic records. Based on the information provided in Jansen (1988), details from the DAMBRK model, and photographs taken during the dam breach, three breach scenarios were conceptualized for the simulations, as illustrated in Figure 1.

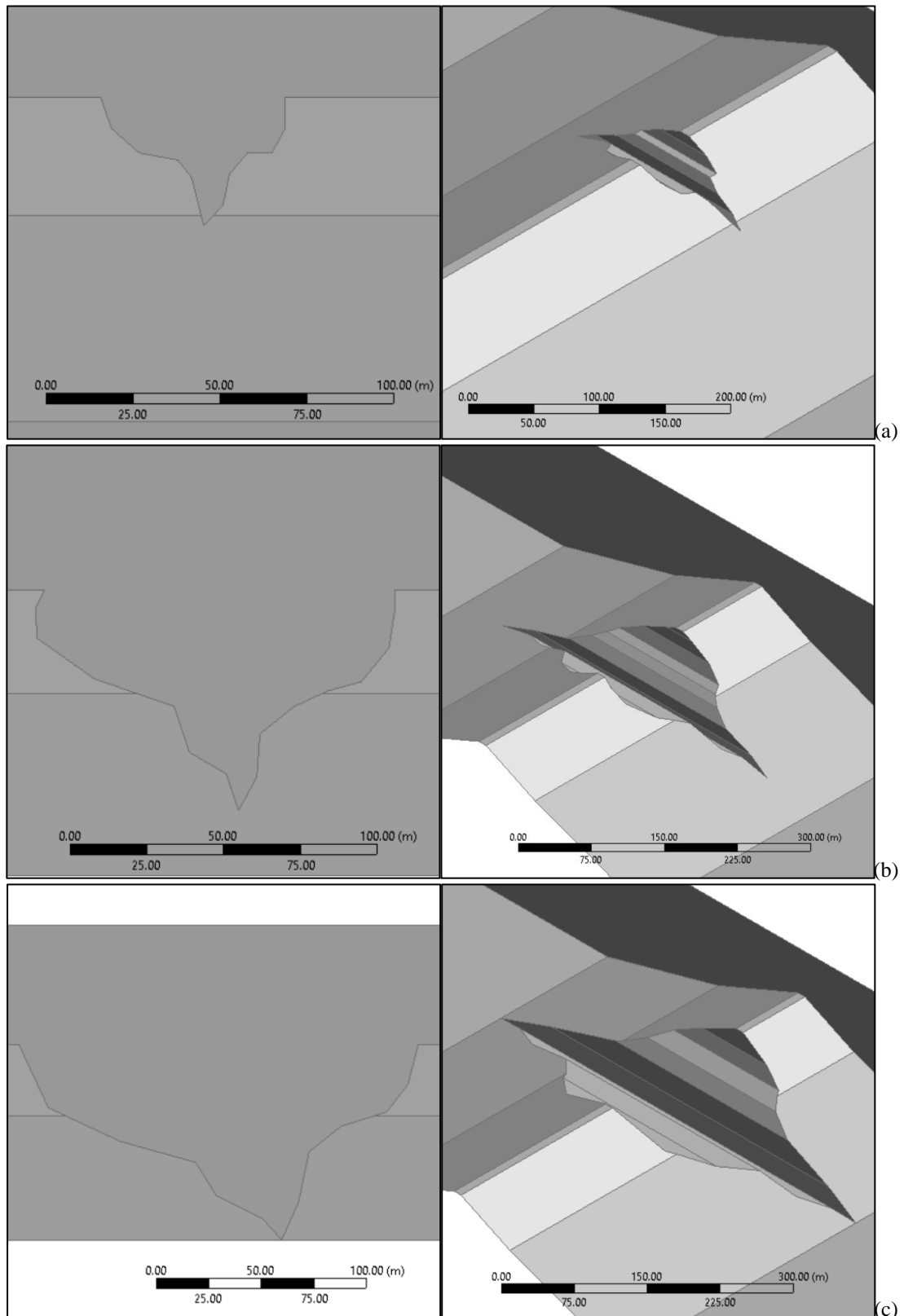


Figure 1: Frontal and isometric views: (a) smaller breach; (b) intermediate breach and (c) larger breach

The computational domain was created with a width of 400 m for the simulations with minor and intermediate dam breaches (Figures 1a and 1b), and 500 m for the simulation with the largest drop (Figure 1c). The projected dam is 516 m long and has a crest length of 10 m, according to data from Jansen (1988). The

simulations were conducted on a computer with the following configuration: 11th Generation Intel(R) Core(TM) i7-1165G7 processor @ 2.80GHz 1.69 GHz and 16GB of RAM installed.

The height from the base to the top of the domain is 200 m for the smaller gap and 150 m for the intermediate and larger gaps. This choice is based on preliminary tests aimed at avoiding numerical reflections and potential numerical acceleration of the air mass between the free surface and the top due to restriction area. The length of the domain upstream of the dam must be extensive enough to establish a free surface without artificial ripples resulting from numerical reflections. After some preliminary tests, a length of 474 m was adopted. The distance from the base of the dam to the outlet is 181 m in the computational domain, for the same reasons related to the upstream section and to ensure a velocity field perpendicular to the outlet. The outlet was considered open, and such a condition is necessary to avoid numerical instabilities.

2.2 Physical-Mathematical Model

The three-dimensional modeling of the problem with the Navier-Stokes equations and mass conservation cannot be performed without employing Reynolds averaging, given the dimensions of the problem, high Reynolds numbers, and computational infeasibility for Direct Numerical Simulation (DNS). Additionally, it is necessary to choose the approach for multiphase simulation, i.e., for water and air. Previous studies conducted by Simões (2012) for 1:1 scale spillways demonstrated that the homogeneous multiphase model tends to calculate a thicker water-air interface for coarser meshes, while the inhomogeneous model, for the same mesh, would calculate a thinner interface. The adoption of the inhomogeneous model is preferable, as convergence analysis for the mesh results in thin interfaces. Based on this observation, the inhomogeneous model was adopted for the present work, described below according to CFX (2021), the software used in this study. Turbulence was modeled using the k-ε model and its original constants (JONES; LAUNDER, 1972).

Equation 1 of the inhomogeneous model corresponds to the principle of mass conservation.

$$\frac{\partial}{\partial t}(r_\alpha \rho_\alpha) + \nabla \cdot (r_\alpha \rho_\alpha \vec{V}_\alpha) = S_{MS\alpha} + \sum_{\beta=1}^{N_p} \Gamma_{\alpha\beta} \quad (1)$$

where, r_α is the volumetric fraction of the alpha phase, such that the sum of r_α for all phases is equal to unity; ρ_α is the density of the alpha phase, \vec{V}_α is the velocity field of the alpha phase, $S_{MS\alpha}$ is a source term and $\Gamma_{\alpha\beta}$ is the mass transfer rate from the beta phase to the alpha phase, per unit volume, N_p is the total number of phases.

The Navier-Stokes equation, belonging to the inhomogeneous model, takes the form of equation 2.

$$\begin{aligned} \frac{\partial}{\partial t}(r_\alpha \rho_\alpha \vec{V}_\alpha) + \nabla \cdot (r_\alpha \rho_\alpha \vec{V}_\alpha \vec{V}_\alpha) = & -r_\alpha \nabla p_\alpha \dots \\ & + \nabla \cdot \left(r_\alpha \mu_\alpha \left(\nabla \vec{V}_\alpha + (\nabla \vec{V}_\alpha)^T \right) \right) + \dots \\ \dots + \sum_{\beta=1}^{N_p} (\Gamma_{\alpha\beta}^+ \vec{V}_\beta - \Gamma_{\beta\alpha}^+ \vec{V}_\alpha) + S_{M\alpha} + M_\alpha \end{aligned} \quad (2)$$

where, p_α is the pressure field of the alpha phase, which is the same for all N_p phases, a necessary condition to close the system of equations; μ_α is the viscosity of the alpha phase; $(\Gamma_{\alpha\beta}^+ \vec{V}_\beta - \Gamma_{\beta\alpha}^+ \vec{V}_\alpha)$ represents the transfer of momentum between phases induced by mass transfer between phases. The term $S_{M\alpha}$ is a source term for the transfer of linear momentum caused by field forces, such as weight force; M_α corresponds to the interfacial forces acting on the α phase due to the presence of the other phases.

2.3 Boundary Conditions, Meshes, and Numerical Methods

The domain's inlet is characterized by a boundary condition imposing a uniform distribution of velocities for water, a distribution of hydrostatic pressures, and a fixed height. It is important to note that this alternative is feasible for the given problem because the governing equations are mixed-type partial differential equations. Although a fixed height is possible, it does not necessarily represent the final height, as its value depends on the influence of the dam and its breach. The domain's outlet was considered open, with zero gradients for the variables. The top was considered open only for air, while the rest of the domain corresponds to a solid boundary modeled with a wall law and a roughness of 2.0 mm.

Ten simulations were conducted, as indicated in Table 2. The selection of these flow rates was done through a trial-and-error process, based on the peak value described in the literature, approximately equal to 66,000 m³/s. The initial flow height at the inlet of 70 m is an initial approximation, as the value for this variable

is part of the problem's solution. The final flow rates, after calculations, were determined by integrating the velocity distribution at the domain's inlet.

Non-structured meshes with tetrahedral elements were employed. Initially, a test was conducted with a mesh of 5,820,514 elements for the larger dam breach, and the result of hydraulic head on the gap's base was compared to the value calculated with a mesh of 729,593 elements. The relative deviation between the results was less than 5%, justifying the adoption of the meshes indicated in Table 2, leading to significant savings in computational time and memory.

Table 2: Information about the inlet boundary condition and adopted meshes

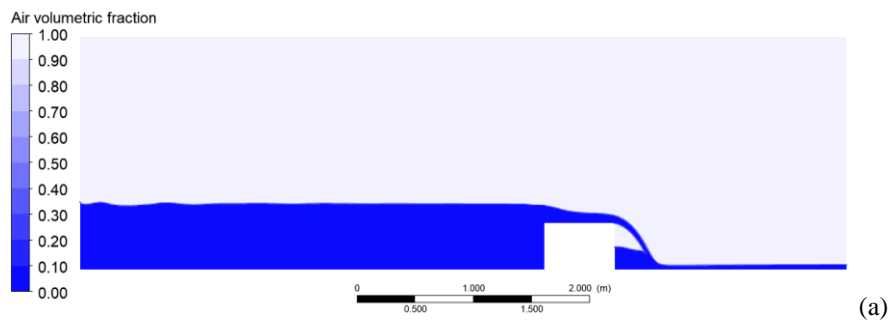
Dam Breach	Flow [m ³ /s]	Width [m]	Inlet velocity [m/s]	Mesh	
				Nodes	Elements
Smaller	9800	400	0.35	1.32E+05	7.42E+05
	5600		0.20	1.32E+05	7.42E+05
	2800		0.10	1.32E+05	7.42E+05
Intermediate	14000		0.50	1.05E+05	5.80E+05
	8400		0.30	1.05E+05	5.80E+05
	2800		0.10	1.05E+05	5.80E+05
Larger	66000	500	1.89	1.31E+05	7.30E+05
	35000		1.00	1.31E+05	7.30E+05
	17500		0.50	1.31E+05	7.30E+05
	49000		1.40	1.31E+05	7.30E+05

The mesh element sizes are similar, but the domains have different dimensions, resulting in meshes with different numbers of elements. The domain for the intermediate dam breach is lower than the domain for the smaller gap, which led to a smaller number of elements in the mesh. This lower height is justified by the fact that lower hydraulic head occur for the intermediate dam breach compared to the smaller dam breach.

For the numerical solution of the equations, the adopted software employs the finite volume method. In its code, there is an option to choose a high-resolution method for the advective part of the equations and for turbulence model equations and this was the choice for the simulations. The convergence criterion is set with residual (RMS) values less than 10^{-4} , and the evolution of results is observed in a pseudo-transient regime as the stopping criterion.

2.4 Modeling analysis using a broad-crested weir

The suitability of the proposed modeling was initially assessed using a broad-crested weir in a two-dimensional domain and experimental data from King (1954). The employed weir has a length of $e = 0.60$ m, a height of 0.40 m, and is situated in a computational domain with dimensions 6.6 m in length and 2.0 m in height. Simulations were conducted with inlet flow rates of 0.110 m³/s, 0.241 m³/s, and 0.731 m³/s using both homogeneous and inhomogeneous multiphase models, and the $k-\epsilon$ turbulence model. As shown in Figure 2, which compares the hydraulic head upstream of the weir calculated with CFD and obtained experimentally, there is agreement between modeling and experimentation, with the results being more consistent for the inhomogeneous model.



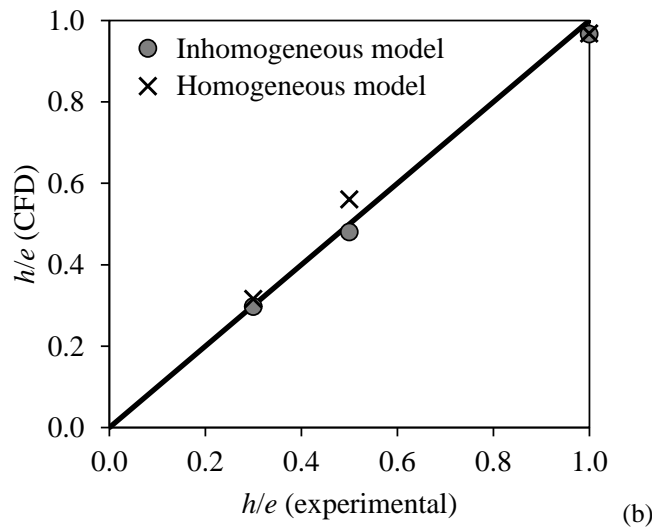


Figure 2: Identification of the free surface for $Q = 0.110 \text{ m}^3/\text{s}$ and the inhomogeneous model (a); comparison between experimental and simulated data with homogeneous and inhomogeneous multiphase models and the $k-\epsilon$ turbulence model (b).

III. RESULTS AND DISCUSSION

The interpretation of numerical results can be facilitated by various types of graphs. For this study, it is essential to understand the position of the free surface upstream of the breaches to calculate the hydraulic head and its relationship with the flow through the breach. The graphs in Figure 3 represent the simulated maximum flow rates for each breach and were generated with the free surface position defined with a volumetric air fraction of 90%, a condition commonly used to identify the water-air interface on spillways studies.

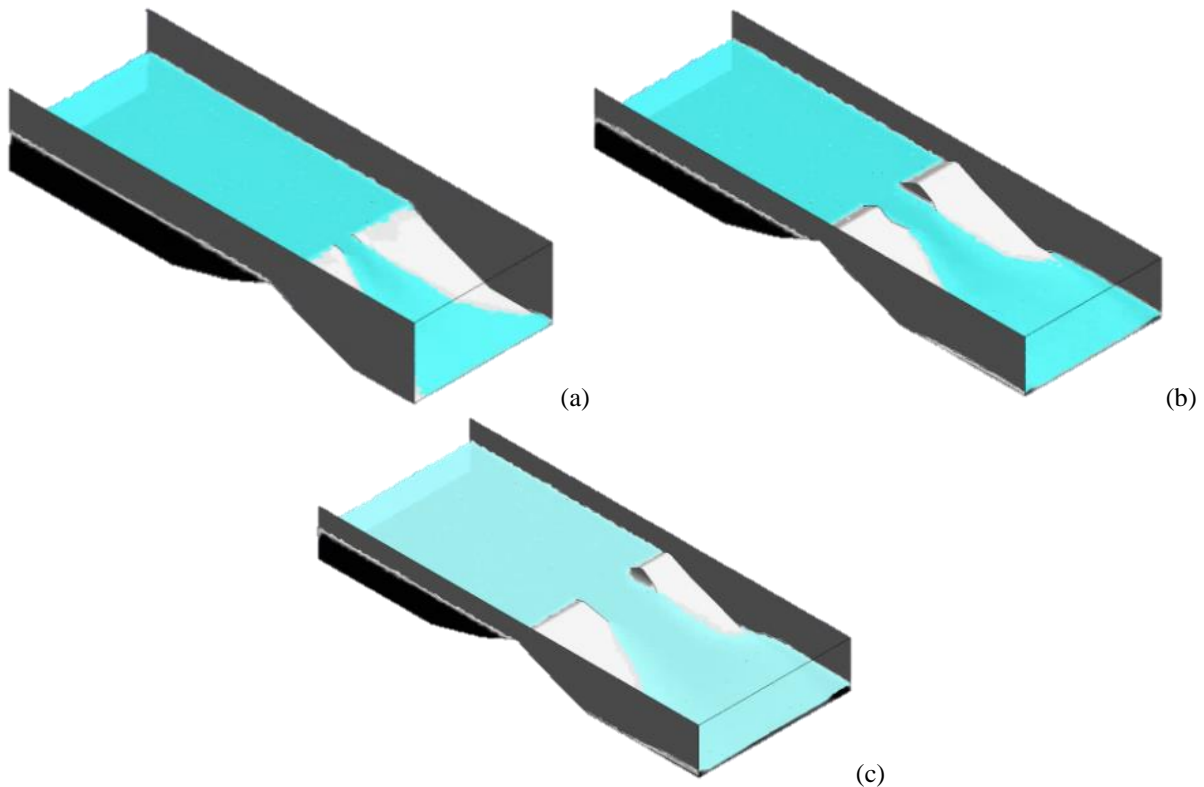


Figure 3: Free surface position, considering the maximum flow rates for each case: (a) smaller dam breach; (b) intermediate; (c) larger dam breach.

The calculations required two weeks of processing time, considering all the tests related to the meshes. As a result, for each case, the flow height in the elements adjacent to the inlet took on the value corresponding to the solution of the problem, differing from the preliminary estimate indicated in Table 1. The flow rate at the inlet also needs to be recalculated by integrating the velocity distribution. To impart a less restrictive character to the results, the flow rates, Q , were divided by the maximum flow rate, $Q_{max} = 65,701 \text{ m}^3/\text{s}$, giving rise to the dimensionless parameter Q/Q_{max} . The hydraulic heads, h , calculated as the height from the free surface to the lowest point of the corresponding dam breach, were dimensionless with respect to the crest width, $b = 10 \text{ m}$, resulting in h/b .

The first analysis considered the behavior of each breach separately and was carried out by calculating the coefficients c_1 and c_2 of the power law expressed by equation 3. Table 3 contains the results for c_1 and c_2 and the correlation coefficient, R , between the values calculated with CFD and equation 3. This information together with the graphs in Figure 4 indicates that there is adherence between the power law and the three-dimensional numerical solution.

$$\frac{Q}{Q_{max}} = c_1 \left(\frac{h}{b}\right)^{c_2} \tag{3}$$

Table 3: Coefficients c_1 and c_2 .

Dam Breach	c_1	c_2	R
Smaller	0.004724	2.48	0.9999
Intermediate	0.002535	2.56	0.9997
Larger	0.001737	2.97	0.9999

The values of c_2 indicate that the smaller breach and the intermediate breach showed behavior similar to that of a triangular weir with a thin or thick wall, whose hydraulic load exponent is equal to 2.5, with relative deviations of 0.8% and 2.4%, respectively. For the largest dam breach, c_2 was greater than 2.5, with a relative deviation of 18.8%.

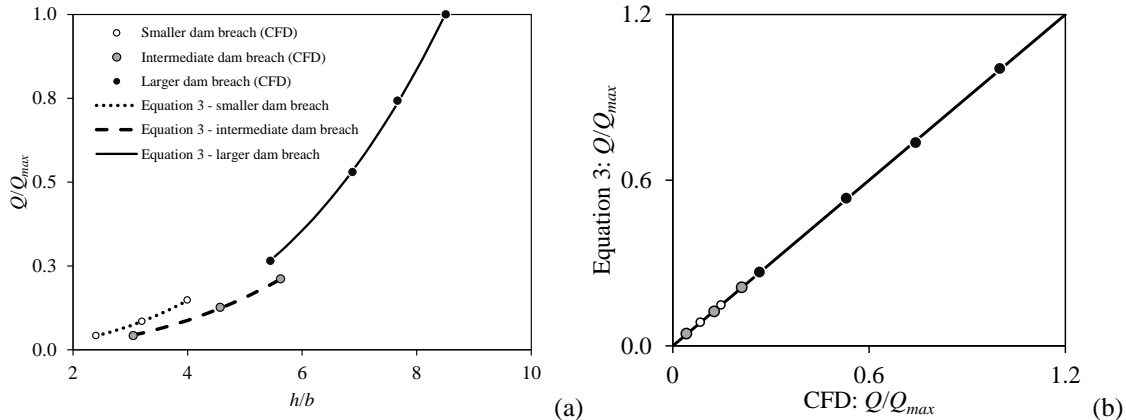


Figure 4: Relationship between dimensionless discharge and hydraulic head (a), and (b) comparison between numerical solution and equation 3.

Assuming that a single equation is sufficient to represent the relationship between flow and hydraulic head for the three dam breaches, equation 4 is proposed, a power law similar to equation 3, but with coefficients different from those indicated in Table 3. The correlation coefficient between numerical results obtained via CFD and those calculated with equation 4 was equal to 0.995. Also noteworthy is the adherence of the points obtained via CFD with the curve generated with equation 4, as indicated in Figure 5.

$$\frac{Q}{Q_{max}} = 0.00133 \left(\frac{h}{b}\right)^{3.09} \tag{4}$$

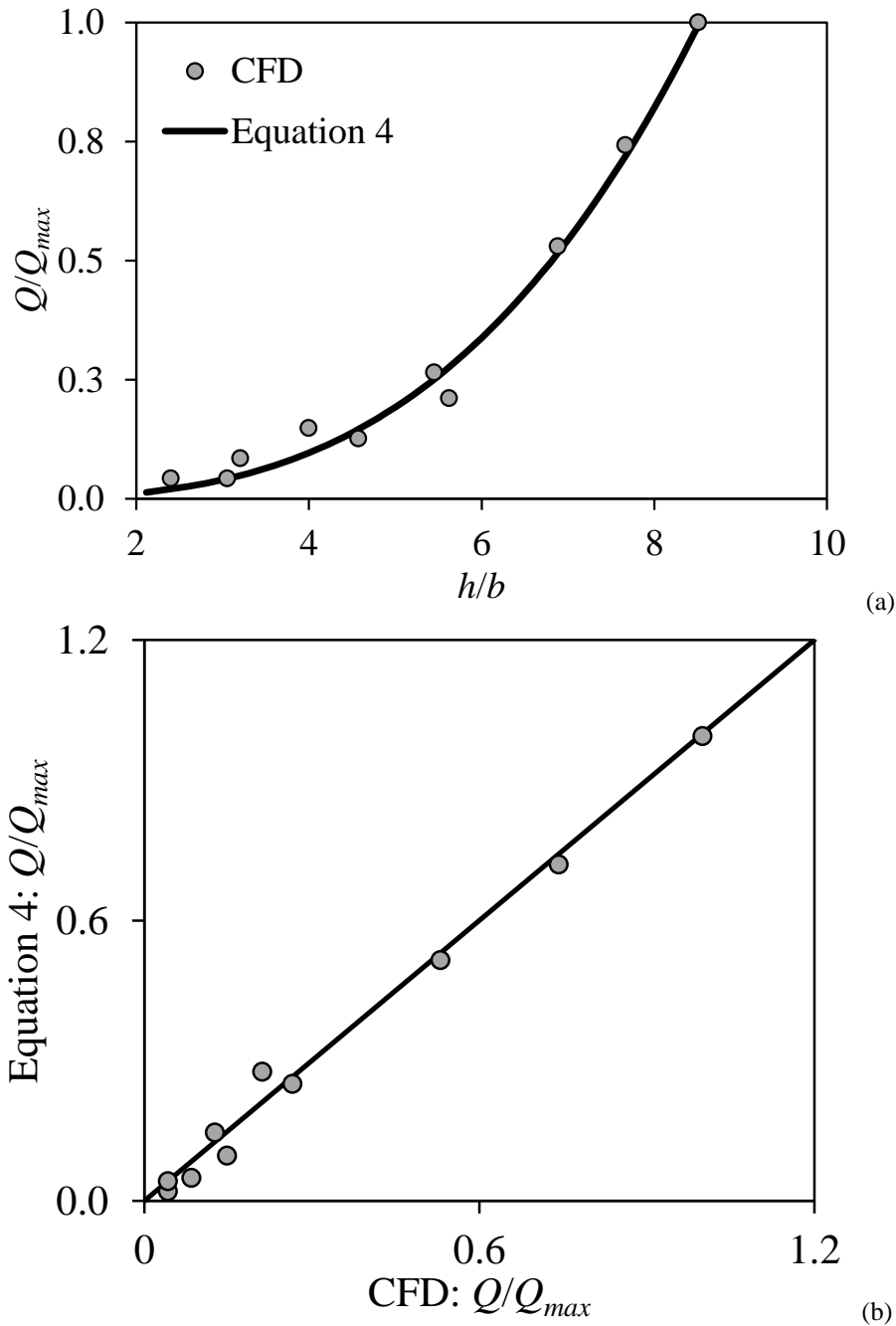


Figure 5: Comparison between equation 4 and CFD results.

IV. CONCLUSION

The results obtained for individual dam breach using the proposed methodology demonstrated the occurrence of exponents (values of c_2) similar to those of triangular and parabolic weirs, forms commonly adopted as approximations for dam breach simulations. Considering only the result for the larger gap, the exponent showed a relative deviation of 18.8% compared to the triangular weir exponent, with a value approximately equal to 3.0. The analysis of all numerical results obtained for the three breaches in an integrated manner resulted in an exponent equal to 3.09, with high correlation and adherence between a power-law and the three-dimensional solutions obtained through computational fluid dynamics. This value corresponds to a relative deviation of 23.6% from the triangular weir value. Experimental studies of 1:1 scale dam breaches are only possible in specific accident situations where monitoring certain variables becomes possible through photographs and limited instrumentation. This work presents solutions that point towards the use of computational fluid dynamics as a methodology to understand the relationship between flow rate and hydraulic head, with the potential to reduce inherent uncertainties in models used for simulations of hypothetical dam break.

ACKNOWLEDGEMENTS

This work was carried out with the support of the Coordination of Superior Level Staff Improvement – Brazil (CAPES) – Financing code 001; processes 88881.708215/2022-01, PDPG Emergencial de Consolidação Estratégica dos Programas de Pós-Graduação (PPGs) stricto sensu acadêmicos com notas 3 e 4, from the Master's Program in Environment, Water, and Sanitation – MAASA – UFBA.

II. REFERENCES

- [1]. Amaral, S.; Caldeira, L.; Viseu, T.; Ferreira, R.M.L. (2020). Designing Experiments to Study Dam Breach Hydraulic Phenomena. *J. Hydraul. Eng.*, 2020, 146(4): 04020014.
- [2]. Biscarini, C; Di Francesco, S.; Manciola, P. (2010). CFD modelling approach for dam break flow studies. *Hydrol. Earth Syst. Sci.*, 14, 705–718, 2010.
- [3]. CFX. CFX Solver Theory. Ansys Canada Ltda., Waterloo, Ontario, 2021.
- [4]. Cristofano, E. A. (1965). Method of Computing Erosion Rate for Failure of Earthfill Dams, Denver, CO (U.S. Bureau of Reclamation).
- [5]. Franca, M.J.; Almeida, A.B. (2004) A computational model of rockfill dam breaching caused by overtopping (RoDaB), *Journal of Hydraulic Research*, 42:2, 197-206.
- [6]. Fread, D. L. (1984a). DAMBRK: The NWS Dam Break Flood Forecasting Model, National Weather Service (NWS) Report, NOAA, Silver Spring, MA.
- [7]. Fread, D. L. (1984b). A Breach Erosion Model for Earthen Dams, National Weather Service (NWS) Report, NOAA, Silver Spring, MA.
- [8]. Froehlich, D. (2008). Embankment Dam Breach Parameters and Their Uncertainties. *Journal of Hydraulic Engineering*, Vol. 134, No. 12, December 1, 2008.
- [9]. Gozali, S.; Hunt, B. (1993). Dam-break solutions for a partial breach. *Journal of Hydraulic Research*, 31(2), 205–214.
- [10]. Hager, W.H.; Schleiss, A. J.; Boes, R. M.; Pfister, M. (2021). *Hydraulic Engineering of Dams*. Taylor & Francis Group, London, UK, 1081 p.
- [11]. Harris, G. W.; Wagner, D. A. (1967). Outflow From Breached Earth Dams, Unpublished B.Sc. Thesis, Department of Civil Engineering, University of Utah, Salt Lake City, UT.
- [12]. Houston, M. (1985). Discussion of Breaching Characteristics of Dam Failures by T. C. MacDonald and J. Langridge-Monopolis, *J. Hydraulic Eng.*, 85, No. HY7,1125-1129.
- [13]. Jansen, R. B., editor (1988). *Advanced Dam Engineering*. New York (Van Nostrand Reinhold).
- [14]. Jones, W.P.; Launder, B.E. (1972). The prediction of laminarization with a two-equation model of turbulence. *International Journal of Heat and Mass Transfer*. 15(2), pp. 301-314.
- [15]. Kaurav, R.; Mohapatra, P. K. (2019). Studying the Peak Discharge through a Planar Dam Breach. *Journal of Hydraulic Engineering*, March 28, 145(6): 06019010, 2019.
- [16]. King, H. W. (1954). *Handbook of hydraulics for the solution of hydraulics problems*. McGraw-Hill, New York, 1954
- [17]. Macdonald, T. C.; Langridge-Monopolis, J. (1984). Breaching Characteristics of Dam Failures, *J. Hydraulic Eng.*, 110, 567-586.
- [18]. Ponce, V. M. (1982). Documented Cases of Earth Dam Breaches, SDSU Civil Eng. Series, No. 82149, 43 p.; San Diego State University, San Diego, CA.
- [19]. Ponce, V. M.; Taher-Shamsi, A.; Shetty, A. V. (2003). Dam-Breach Flood Wave Propagation Using Dimensionless Parameters. *Journal of Hydraulic Engineering*, Vol. 129, No. 10, October 1, 2003.
- [20]. Singh, V. P. (1996). *Dam Breach Modeling Technology*. Baton Rouge, U.S.A., Springer, 242 p.
- [21]. Singh, V. P.; Quiroga, C. A. (1988). Dimensionless analytical solutions for dam-breach erosion. *J. Hydraulic Res.*, 26(2), 179-197.
- [22]. Singh, K. P.; Snorrason, A. (1982). Sensitivity of Outflow Peaks and Flood Stages to the Selection of Dam Breach Parameters and Simulation Models, SWS Contract Report 289, 179 p., Surface Water Section, State Water Survey Division, Illinois Department of Energy and Natural Resources, Champaign, IL.
- [23]. Tabrizi, A.A.; Elalfy, E.; Elkholy, M.; Chaudhry, M. H.; Imran, J. (2017) Effects of compaction on embankment breach due to overtopping. *Journal of Hydraulic Research*, 55:2, 236-247.
- [24]. Tao, H.; Tao, J. (2017). Quantitative analysis of piping erosion micro-mechanisms with coupled CFD and DEM method. *Acta Geotechnica*, 12:573–592.
- [25]. Wahl, T.L. (2004). Uncertainty of predictions of embankment dam breach parameters. *Journal of Hydraulic Engineering*, 130(5), 389–397.
- [26]. Wetmore, J. N.; Fread, D. L. (1984). The NWS Simplified Dam Break Flood Forecasting Model for Desk-Top and Hand-Held Microcomputers, National Weather Service Report, NOAA, Silver Spring, MA.
- [27]. Wurbs, R.A. (1987). Dam-breach flood wave models. *Journal of Hydraulic Engineering*, 113(1), 29–46; 114(5), 565–569.